



ACADEMIC
PRESS

Available online at www.sciencedirect.com

SCIENCE @ DIRECT®

Journal of Magnetic Resonance 162 (2003) 46–53

JMR
Journal of
Magnetic Resonance

www.elsevier.com/locate/jmr

Phase-modulated heteronuclear decoupling in NMR of solids

A.K. Khitrin,^a Toshimichi Fujiwara,^b and Hideo Akutsu^{b,*}

^a Department of Chemistry, Kent State University, Kent, OH 44242-0001, USA

^b Institute for Protein Research, Osaka University, 3-2 Yamadaoka, Suita, Osaka 565-0871, Japan

Received 26 April 2002; revised 14 November 2002

Abstract

A theoretical description of heteronuclear decoupling in solids, which takes into account homonuclear dipole–dipole interactions and spinning of the sample, is presented. Based on this analysis, a simple and efficient decoupling sequence n PPM is introduced. It consists of $n/4$ TPPM subcycles, followed by another $n/4$ subcycles with reversed phases.

© 2003 Elsevier Science (USA). All rights reserved.

Keywords: Heteronuclear decoupling; Decoupling in solids; Spinning rate; Phase modulation; TPPM

1. Introduction

Heteronuclear decoupling is one of the main components of high-resolution NMR. A spectrum of one type of nuclei can often be significantly improved when interactions with nuclei of other types are suppressed. Decoupling increases both resolution and sensitivity. For many applications, especially multi-dimensional, enhanced sensitivity is the most important result and goal of efficient decoupling. Therefore, in this work the height of decoupled peak is used as a quantitative measure of the decoupling efficiency. To be more specific, we are talking about ^1H as the abundant (I) and ^{13}C as the rare nuclei (S), though the presented analysis is quite general.

In liquids, a distribution of proton chemical shifts made it necessary to search for broadband decoupling schemes. The first of such schemes was the noise decoupling, proposed by Ernst [1]. Levitt and Freeman [2] introduced an efficient scheme with composite pulses. A mechanism of decoupling in liquids is relatively simple and can be analyzed with the dynamics of a single spin I . A detailed theory was presented by Waugh [3]. Later, it was extended to systems of arbitrary spins I [4]. Improved understanding of the underlying spin dynamics facilitated development of decoupling techniques. Very

efficient broadband decoupling sequences for liquids, such as MLEV-16 [5], WALTZ-16 [6], GARP [7], frequency-switched composite pulses [8], and the adiabatic frequency sweep [9] have been introduced and are commonly used now.

Homonuclear dipolar interactions between spins I in solids and liquid crystals result in correlated dynamics of a large number of spins and complicate the physical picture of decoupling. For liquid crystals, where RF heating [10] makes it necessary to use low decoupling power, several broadband decoupling sequences had been proposed [11–13].

Progress in heteronuclear decoupling in solids was extremely slow. CW irradiation remained the main decoupling technique until the two-pulse phase modulation (TPPM) sequence was introduced by Bennett et al. [14]. This sequence offered a simple way to decouple better than with CW irradiation and stimulated a number of studies on the factors which influence decoupling [15] as well as new decoupling schemes [16–22] and their applications [23–25]. Though the new sequences, CPM m - n [21] or SPINAL-64 [13], perform noticeably better than TPPM at low to moderate spinning rates [25], the problem of heteronuclear decoupling in solids is still far from a satisfactory solution. One of the major reasons is the absence of reliable theoretical tools for handling this problem. Analytical perturbative approaches, such as the average Hamiltonian theory of Waugh [26], require a small parameter, which is a ratio

* Corresponding address. Fax: +81-6-6879-8599.

E-mail address: akutsu@protein.osaka-u.ac.jp (H. Akutsu).

of the magnitude of the interaction, in frequency units, and the frequency with which this interaction is modulated. Under experimental decoupling conditions, this parameter is not small. In addition, even if the average Hamiltonian could be calculated with high accuracy, it is not easier to calculate spin dynamics with this Hamiltonian than with initial dipolar interactions.

Though there have been reports on using an amplitude modulation of the decoupling field [19,27], we believe that phase modulation is the most economic way of using available RF power and discuss in this work only the phase-modulation decoupling techniques. In the following theoretical section we avoided any detail calculations and focused on presenting a consistent qualitative picture of decoupling in solids. Since a detailed description of the proton spins' motion is not available, this motion is represented by some unknown correlation function or spectral density, and the effects of the RF field and the sample spinning are explicitly separated. This is achieved by considering the proton spin dynamics in several different frames.

2. Theory

The aim of this section is to answer the following questions: (1) why does the CW decoupling work so well in solids; (2) how the TPPM increases the efficiency of decoupling; and (3) how can some other types of phase modulation give further improvement? The first question does not appear so simple if one takes into consideration strong dipolar interactions between protons. Without decoupling ^{13}C linewidth in organic solids is conservatively estimated at several kHz. Application of an RF field, with an amplitude comparable to the dipolar linewidth of protons, reduces the ^{13}C linewidth to tens of Hz, producing, therefore, a line narrowing by two orders of magnitude.

2.1. CW decoupling

We start our discussion of the CW decoupling with the secular Hamiltonian in the rotating frame:

$$\mathcal{H} = -\omega_{\text{rf}}I_x + \mathcal{H}_{\text{IS}} + \mathcal{H}_{\text{dz}}, \quad (1)$$

where

$$\mathcal{H}_{\text{IS}} = \sum_{j>0} 2b_{0j}S_{0z}I_{jz} \quad (2)$$

and

$$\mathcal{H}_{\text{dz}} = \sum_{i>j>0} b_{ij}(2I_{iz}I_{jz} - I_{ix}I_{jx} - I_{iy}I_{jy}) \quad (3)$$

are the interactions between the ^{13}C spin S_0 and surrounding protons I_j and the homonuclear dipolar interaction between the protons, respectively. Sometimes

this frame is called the doubly rotating frame, since it is the rotating frame for both types of nuclei. However, we reserve the term double rotating frame for the frame which performs additional rotation for the proton spins. For an isolated I – S pair, the cross term between chemical-shielding anisotropy and heteronuclear dipolar coupling strongly affects the decoupling [28]. Homonuclear dipole–dipole interactions make this effect less pronounced [28], and the chemical-shielding anisotropy is not taken into account in our theoretical description.

The quality of decoupling is determined by the rate of dephasing of the ^{13}C spin S . The dephasing is caused by the local field h_z , created by the surrounding protons:

$$h_z = \sum_{j>0} 2b_{0j}I_{jz}. \quad (4)$$

When the decoupling is good, the dephasing rate is small, and the transverse component of the spin S decays exponentially:

$$\langle S_x(t)S_x(0) \rangle \propto \exp(-t/T_2^*). \quad (5)$$

To find the characteristic time T_2^* of the S spin decay signal, one can use an expansion at $t \ll T_2^*$:

$$\begin{aligned} \exp(-t/T_2^*) &\approx 1 - t/T_2^* \approx \langle \cos[\varphi(t)] \rangle \\ &\approx 1 - (1/2)\langle \varphi^2(t) \rangle \\ &= 1 - (1/2)\left\langle \left(\int_0^t h_z(t_1)dt_1 \right)^2 \right\rangle \\ &= 1 - (1/2) \int_0^t \int_0^t dt_1 dt_2 \langle h_z(t_1)h_z(t_2) \rangle, \quad (6) \end{aligned}$$

where $\varphi(t)$ is the phase, acquired by the spin S under the influence of the local field $h_z(t)$. Therefore,

$$1/T_2^* = (1/2t) \int_0^t \int_0^t dt_1 dt_2 \langle h_z(t_1)h_z(t_2) \rangle. \quad (7)$$

When the Hamiltonian \mathcal{H} is time-independent,

$$\begin{aligned} \langle h_z(t_1)h_z(t_2) \rangle &= \text{Tr}\{\exp(i\mathcal{H}t_1)h_z \exp(-i\mathcal{H}t_1) \\ &\quad \times \exp(i\mathcal{H}t_2)h_z \exp(-i\mathcal{H}t_2)\} \\ &= \text{Tr}\{\exp[i\mathcal{H}(t_1 - t_2)]h_z \exp[-i\mathcal{H}(t_1 - t_2)]h_z\} \\ &= \langle h_z(\tau)h_z(0) \rangle \equiv g(\tau), \quad (8) \end{aligned}$$

where $\tau = t_1 - t_2$. In this case, when the correlation function of the local field $g(\tau)$ decays much faster than T_2^* , one can obtain from (Eq. (7)) that

$$\begin{aligned} 1/T_2^* &= s(0), \text{ where} \\ s(\omega) &= (1/2) \int_{-\infty}^{\infty} \exp(i\omega\tau)g(\tau)d\tau \quad (9) \end{aligned}$$

is the spectral density of the local field. This spectral density is shown schematically in Fig. 1 and is discussed in more details below.

MAS with the frequency ω_r creates an additional modulation of the local field at the frequencies $\pm\omega_r$ and $\pm 2\omega_r$ caused by a time dependence of the dipolar

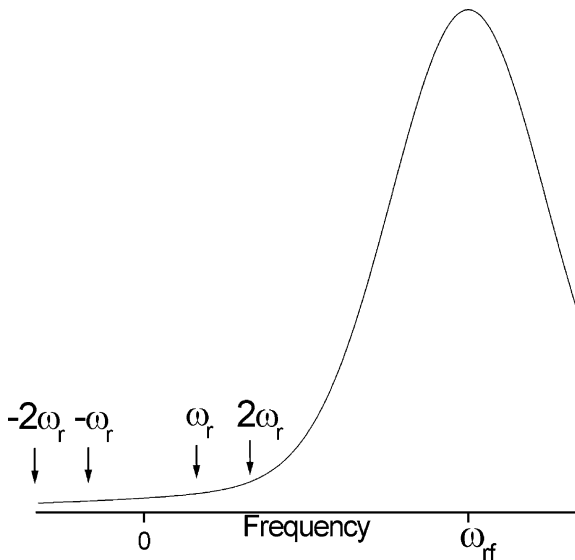


Fig. 1. Spectral density of the local field.

constants b_{0j} in (Eq. (4)). Then, instead of a single contribution at $\omega = 0$, relaxation of the ^{13}C spin is determined by the spectral density at the frequencies $\pm\omega_r$ and $\pm 2\omega_r$:

$$\begin{aligned} 1/T_2^* &= \frac{1}{2}a_1[s(\omega_r) + s(-\omega_r)] \\ &+ \frac{1}{2}a_2[s(2\omega_r) + s(-2\omega_r)], \end{aligned} \quad (10)$$

where the coefficients a_1 and a_2 ($a_1 + a_2 = 1$) depend on the orientation of the carbon-proton internuclear vectors to the rotor axis and can be calculated for each particular structure. Powder average for a single internuclear vector gives $a_1/a_2 = \sqrt{2}$.

To separate the contributions of the RF field and the dipolar interactions to $s(\omega)$, it is convenient to use the double rotating frame for the proton spins: the frame which rotates around the x -axis of the rotating frame with the frequency ω_{rf} . The corresponding unitary transformation is

$$\rho' = U\rho U^{-1}, \quad U = \exp(-i\omega_{\text{rf}}I_x t), \quad (11)$$

where ρ and ρ' are the density matrices in the rotating and the double rotating frames, respectively. By performing this transformation, we can find that

$$g(\tau) = g'(\tau) \cos(\omega_{\text{rf}}\tau), \quad (12)$$

where the correlation function $g'(\tau)$ is determined by the dipolar interactions in the double rotating frame. Therefore, the spectral density in the rotating frame (Eq. (9)) is a superposition of the two shapes. One of them is obtained from the spectral density in the double rotating frame $s'(\omega)$ by a $+\omega_{\text{rf}}$ shift and another one is obtained by a ω_{rf} shift. Since they give the same contribution to $1/T_2^*$, we can further consider only one of the components, for example, the one with the $+\omega_{\text{rf}}$ shift. By rewriting the dipolar interaction (Eq. (3)) as

$$\mathcal{H}_{\text{dz}} = -(1/2)\mathcal{H}_{\text{dx}} + \mathcal{H}^2 + \mathcal{H}^{-2}, \quad (13)$$

where $\mathcal{H}^{\pm 2}$ are defined with respect to the x -axis of the rotating frame, we will find that the Hamiltonian in the double rotating frame is

$$\mathcal{H}' = -(1/2)\mathcal{H}_{\text{dx}} + \mathcal{H}^2 \exp(2i\omega_{\text{rf}}t) + \mathcal{H}^{-2} \exp(-2i\omega_{\text{rf}}t). \quad (14)$$

The periodic oscillating terms can be replaced by the average or effective Hamiltonian \mathcal{H}_{eff} :

$$\mathcal{H}'' = -(1/2)\mathcal{H}_{\text{dx}} + \mathcal{H}_{\text{eff}}. \quad (15)$$

The first term of the expansion of the effective Hamiltonian in $\omega_{\text{loc}}/\omega_{\text{rf}}$, where $\omega_{\text{loc}}^2 = \text{Tr}(\mathcal{H}_{\text{dz}}^2)/\text{Tr}(I_z)^2$, is [29]

$$\mathcal{H}_{\text{eff}}^{(1)} = (1/2\omega_{\text{rf}})[\mathcal{H}^2, \mathcal{H}^{-2}]. \quad (16)$$

Since we are interested in the tails of the spectra, the first term of the expansion is not sufficient but gives some information about the magnitude and symmetry of \mathcal{H}_{eff} .

The spectral density $s(\omega)$ resembles an NMR absorption line in the rotating frame or, more precisely, the Fourier transform of the real part of the FID signal (the correlator $\langle I_z(t)I_z(0) \rangle$). These spectra would be exactly proportional to one another if the dipolar constants b_{0j} of interaction with near protons are all equal, or if there is no correlation in the motion of the spins of these neighbor protons. Both of these assumptions are not too good for real structures, but this analogy is useful for better understanding what type of correlator we are dealing with. The spectrum $s(\omega)$ is schematically represented in Fig. 1. As it was explained above, only one of the halves of the spectrum is shown. The central part of the spectrum (near ω_{rf}) and the near tails, determined by the term $-(1/2)\mathcal{H}_{\text{dx}}$ (Eq. (15)), resemble a Gaussian curve. Far tails are primarily due to \mathcal{H}_{eff} and are approximately Lorentzian. Relaxation of the ^{13}C spin is determined by the amplitudes of $s(\omega)$ at the frequencies $\pm\omega_r$ and $\pm 2\omega_r$ according to Eq. (10).

At high-spinning rates, one more factor should be taken into account. Similar to ordinary proton spectrum in the laboratory frame under fast MAS, the spectral density in the rotating frame will display spinning sidebands, due to modulation of the $-(1/2)\mathcal{H}_{\text{dx}}$ term of the Hamiltonian (Eq. (15)). Instead of the shape schematically shown in Fig. 1, $s(\omega)$ will have multiple local maxima and minima. For better decoupling, the frequencies $\pm\omega_r$ and $\pm 2\omega_r$ should coincide with the minima, i.e., lie in the middle between the spinning sidebands. When the frequencies $\pm\omega_r$ and $\pm 2\omega_r$ coincide with the spinning sidebands, the decoupling is spoiled. These conditions can be written as

$$\omega_{\text{rf}}/\omega_r = k + 1/2, \quad k = 0, 1, 2, \dots, \quad (17a)$$

and

$$\omega_{\text{rf}}/\omega_r = k, \quad k = 1, 2, \dots \quad (17b)$$

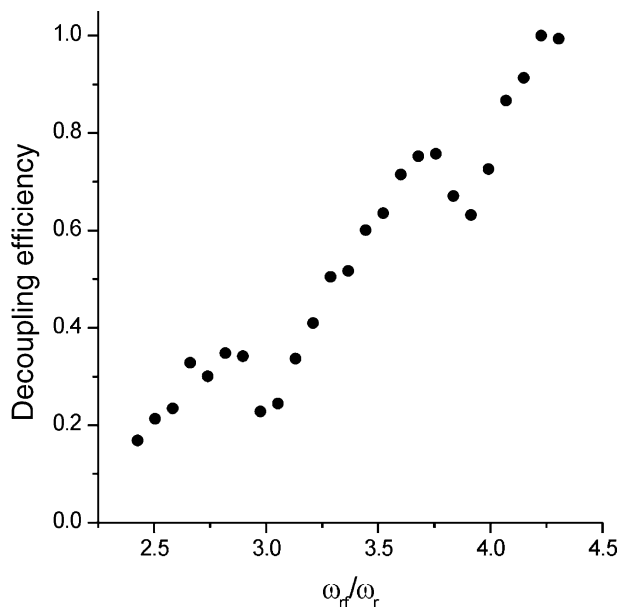


Fig. 2. Dependence of the CW decoupling efficiency in glycine on the ratio between the RF power and the spinning rate. The spinning rate is 23.0 kHz.

The condition (a) is favorable for the resonance CW decoupling, while the condition (b) is unfavorable.

Fig. 2 shows the experimental dependence of the CW decoupling performance in glycine (relative height of the ^{13}C peak of the CH_2 group) at the spinning rate $\omega_{\text{r}}/2\pi = 23.0$ kHz. One can see distinct minima at $\omega_{\text{rf}}/\omega_{\text{r}} = 3$ and 4. At higher spinning rates this effect will be more pronounced, and one needs to consider the conditions (Eqs. (17a),(17b)) for optimizing the decoupling efficiency. The decrease in decoupling efficiency at integer ratios of $\omega_{\text{rf}}/\omega_{\text{r}}$ has been attributed to a rotary-resonance recoupling [30]. However, the rotary resonance could explain the decreased decoupling efficiency only for $\omega_{\text{rf}}/\omega_{\text{r}} = 1$ or 2.

To conclude the discussion of the CW decoupling, we would like to mention that its extremely high performance is based on the two factors: the symmetry of the proton–proton dipolar interactions, which have no $\mathcal{H}^{\pm 1}$ terms with respect to the RF field direction in the rotating frame, and fast decaying tails of the dipolar lineshapes in solids.

2.2. TPPM decoupling

When the phase Φ of the RF field is modulated, the interaction with this field in the rotating frame is

$$\mathcal{H}_{\text{rf}} = -\omega_{\text{rf}}I_x \cos[\Phi(t)] - \omega_{\text{rf}}I_y \sin[\Phi(t)]. \quad (18)$$

If the phase is small ($\cos \Phi \approx 1$, $\sin \Phi \approx \Phi$), the modulation is equivalent to an additional field, applied along the y -axis of the rotating frame. Since both \mathcal{H}_{IS} and \mathcal{H}_{dz} (Eqs. (1)–(3)) are invariant with respect to rotations around the z -axis, it is more convenient to perform the

exact transformation to the frame, where the RF field is time-independent and aligned along the x -axis. The Hamiltonian in this toggling frame is

$$\mathcal{H} = -\omega_{\text{rf}}I_x - f(t)I_z + \mathcal{H}_{\text{IS}} + \mathcal{H}_{\text{dz}}. \quad (19)$$

The only difference with the Hamiltonian (Eq. (1)) is the additional field $f(t) = -d\Phi/dt$ in z -direction. The transformation to this frame is a generalization of the transformation to the rotating frame, usually performed to make the in-resonance component of the RF field time-independent. Experimentally, the phase is changed stepwise. Then, the effect of such phase modulation in the toggling frame is a sequence of δ -pulses in $\pm z$ direction. As an example, for the TPPM sequence [14], when the cycle consists of two pulses, with duration τ each and phases $+\Phi_0$ and $-\Phi_0$,

$$f(t) = 2\Phi_0 \sum_{k=0}^{\infty} \{\delta(t - (2k+1)\tau) - \delta(t - 2k\tau)\}. \quad (20)$$

In the double rotating frame, which rotates with the frequency $\omega_{\text{m}} = \pi/\tau$ around the x -axis of the toggling frame, the Hamiltonian for the proton spins can be written as

$$\mathcal{H}'' = (\omega_{\text{m}} - \omega_{\text{rf}})I_x + 2\Phi_0 I_z \sum_{k=0}^{\infty} \delta(t - k\tau) - (1/2)\mathcal{H}_{\text{dz}} + \mathcal{H}_{\text{eff}}. \quad (21)$$

Compared to the case of CW decoupling (Eq. (15)), there are additional fields along the x and z -axis of the double rotating frame. At $\omega_{\text{loc}}\tau \ll 1$ one can replace the z -field by its average value $\omega_z = 2\Phi_0/\tau$. Then, the Hamiltonian [21] becomes

$$\mathcal{H}'' = \omega_x I_x + \omega_z I_z - (1/2)\mathcal{H}_{\text{dz}} + \mathcal{H}_{\text{eff}}, \quad (22)$$

where $\omega_x = \omega_{\text{m}} - \omega_{\text{rf}}$. It should be noted, that this is an approximation, which corresponds to neglecting higher harmonics of the TPPM and replacing the stepwise phase modulation by a harmonic one ($\Phi(t) \propto \cos(\omega_{\text{m}}t)$). In practice, TPPM and the cosine phase modulation show very close performance (though not exactly the same). In what follows, we will make no difference between them and use the Hamiltonian (Eq. (22)) for explaining the mechanism of the TPPM decoupling.

The Hamiltonian (Eq. (22)) suggests that the improved performance of the TPPM is created by an off-resonance irradiation in the rotating frame. This off-resonance irradiation produces an asymmetric distortion of the spectral density and decreases its low-frequency tail. However, this mechanism alone is insufficient to explain high-experimental efficiency of the TPPM. Another factor to be considered is the partial averaging of the dipolar interactions by the effective field. Under typical experimental conditions, the effective field in the double rotating frame is comparable to the residual dipolar interactions and is capable of producing some averaging effect. If averaging is the

main factor that determines the improved decoupling, then the TPPM would perform equally well for $\omega_m < \omega_{rf}$ ($\omega_{rf}\tau > 180^\circ$). In practice, however, it works well only for $\omega_m > \omega_{rf}$ ($\omega_{rf}\tau < 180^\circ$). Therefore, high-decoupling efficiency of the TPPM is due to the combined action of both asymmetric distortion of the spectral density and partial averaging of the dipolar interactions in the double rotating frame.

2.3. Other forms of small-angle phase modulation

The effective field in the double rotating frame produces the best averaging of the dipolar interactions when it is at the magic angle with the x -axis. This condition, $|\omega_z/\omega_x| = \sqrt{2}$, is realized at four different combinations of sign of ω_z and ω_x . As it was discussed above, only two of these orientations, with $\omega_x = \omega_m - \omega_{rf} > 0$, are good for decoupling. By switching the direction of the effective field between these two orientations, one can achieve better averaging of the dipolar interaction. The time interval between the switches should correspond to a 2π precession around the effective field. The mechanism of this additional averaging is the same as in the frequency-switched Lee-Goldburg (FSLG) experiment [31]. The change in the direction of the effective field also mixes the locked (parallel to the effective field) and unlocked spin components. This moves the low-frequency component of the spectral density to higher frequencies. Therefore, a periodic change of the sign of ω_z can enhance both of the mechanisms, responsible for high performance of the TPPM sequence.

Practically, such change of the ω_z sign can be realized by the n -pulse sequence, which consists of $n/4$ TPPM subcycles (τ, Φ_0) , $(\tau, -\Phi_0)$, followed by another $n/4$ subcycles $(\tau, -\Phi_0)$, (τ, Φ_0) with reversed phases, where (τ, Φ) is the pulse of duration τ and phase Φ . In analogy with the TPPM, we abbreviated this new pulse sequence n PPM. As an example, a 32PPM sequence $[(\tau, \Phi_0), (\tau, -\Phi_0)]_8 [(\tau, -\Phi_0), (\tau, \Phi_0)]_8$ with the pulses flip angle $\omega_{rf}\tau = 167^\circ$ and the phase excursion angle $2\Phi_0 = 18.3^\circ$ performs 2π rotation in the double rotating frame around the effective field (which is at the magic angle with the x -axis) and then, another 2π rotation around the new direction of the effective field. The experimental results for this pulse sequence are presented in the next section.

Instead of a sudden change of the effective field direction, one can change it smoothly in a harmonic way. The following phase-modulation function can be used:

$$\Phi(t) = \Phi_0 \cos(\omega_m t) \cos(\omega_{m1} t), \quad (23)$$

where ω_{m1} is the frequency of the change of direction of the effective field in the double rotating frame and $\omega_{m1} \ll \omega_m$. By rewriting the product of cosines as a sum of cosine terms, we will find that this sequence (Eq. (23)) is equivalent to the CPM 2- n decoupling sequence. Se-

quences CPM m - n have been introduced earlier [21] and employ the phase-modulation function, which is a sum of m cosine terms with equal amplitudes and frequency intervals ω_{rf}/n between the harmonics. Sequences with a larger number of harmonics perform a more complicated motion of the effective field in the double rotating frame. The results for one of these sequences, CPM 4-7, will be shown for comparison in the experimental section. The phase-modulation function of the CPM 4-7 decoupling sequence is

$$\Phi(t) = (1/7)\{-\cos[(6/7)\omega_{rf}t] + \cos[\omega_{rf}t] + \cos[(8/7)\omega_{rf}t] - \cos[(9/7)\omega_{rf}t]\}. \quad (24)$$

3. Results and discussion

In ^{13}C CPMAS spectra, a high-spinning rate is needed to suppress spinning sidebands and increase intensities of central peaks. For the samples used in this work and the ^{13}C resonance frequency 125 MHz, a spinning rate of about 12 kHz was sufficient. At this spinning rate, spinning sidebands are small, and further increase of the spinning rate does not increase the intensities of central peaks.

Fig. 3 shows the relative performance of TPPM, CPM 4-7, and 32PPM at 12.0 kHz spinning rate as a function of the decoupling power (γB_2). For each of the sequences the adjustable parameters were independently optimized for each value of the decoupling power. The sample, glycine, is a suitable model because it has only two different carbons and, consequently, provides strong

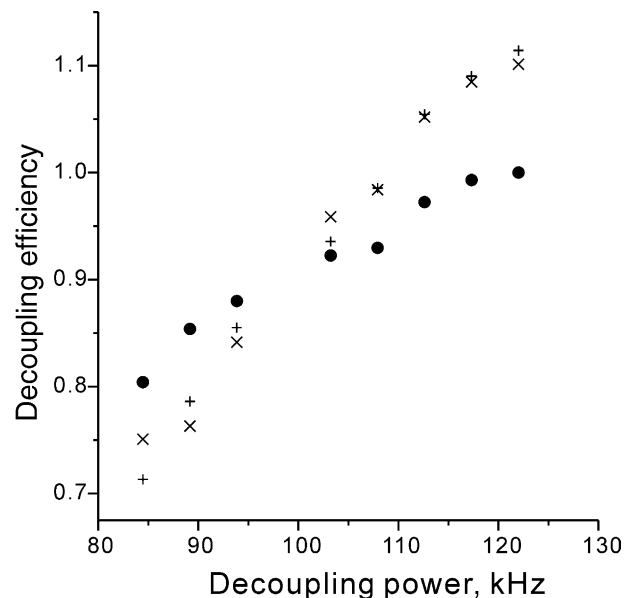


Fig. 3. Decoupling efficiency in glycine of TPPM (●), CPM 4-7 (+), and 32PPM (×) as a function of the decoupling power. The spinning rate is 12.0 kHz.

signals even at natural isotope abundance. At the same time, the ^{13}C of the CH_2 group is strongly coupled to the protons and presents a good test case for decoupling. The height of the CH_2 peak was used as a quantitative measure of decoupling efficiency. Clearly, at decoupling powers above 100 kHz, a noticeable improvement over TPPM can be obtained.

An improved performance is not the only advantage of the 32PPM sequence. Its efficiency has much better dependence on the experimentally adjustable parameters τ and Φ_0 . This facilitates a search of optimum parameters, especially when signals are weak. Fig. 4 shows the dependence of the TPPM and 32PPM decoupling efficiency on the phase excursion angle $2\Phi_0$. With the decoupling power of 117 kHz and spinning rate of 12 kHz, the peak performance of TPPM is reached at $\tau = 4.0 \mu\text{s}$ and $2\Phi_0 = 10^\circ$. Fig. 4 is a one-dimensional slice through a two-dimensional plane of parameters, which intersects this point. The decoupling efficiency of the 32PPM has a single broad maximum, in contrast to multiple local maxima of the TPPM. This maximum is reached at parameter values which are very close to theoretical ($\omega_{\text{rf}}\tau = 167^\circ$, $2\Phi_0 = 18^\circ$).

Experimental ^{13}C spectra of two different samples, valine and glycine, were obtained with 32PPM and TPPM decoupling at the same parameters values (Fig. 5). The enhancement of peak heights (>10%) for all carbons illustrates the additional averaging produced by the 32PPM sequence.

With a larger number of adjustable parameters, one can build more flexible sequences with potentially higher performance. In this sense, the TPPM is always better

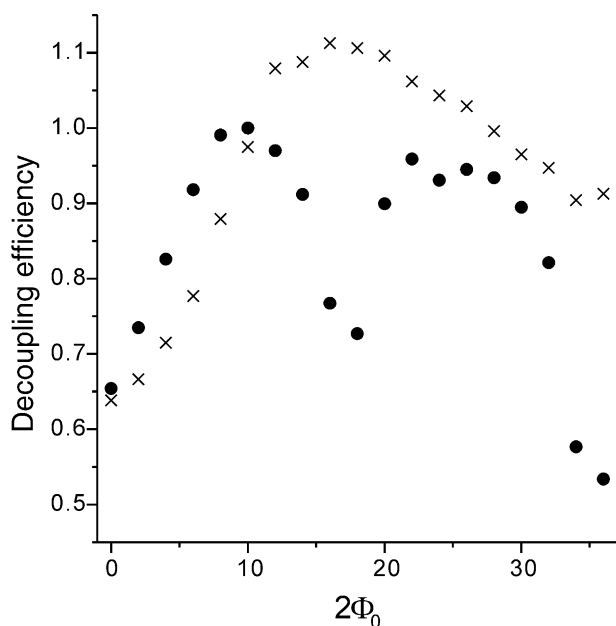


Fig. 4. Decoupling efficiency in glycine of TPPM (●) and 32PPM (×) as a function of the phase excursion angle $2\Phi_0$ at 12.0 kHz spinning rate, 117 kHz decoupling power, and 4.0 μs pulses.

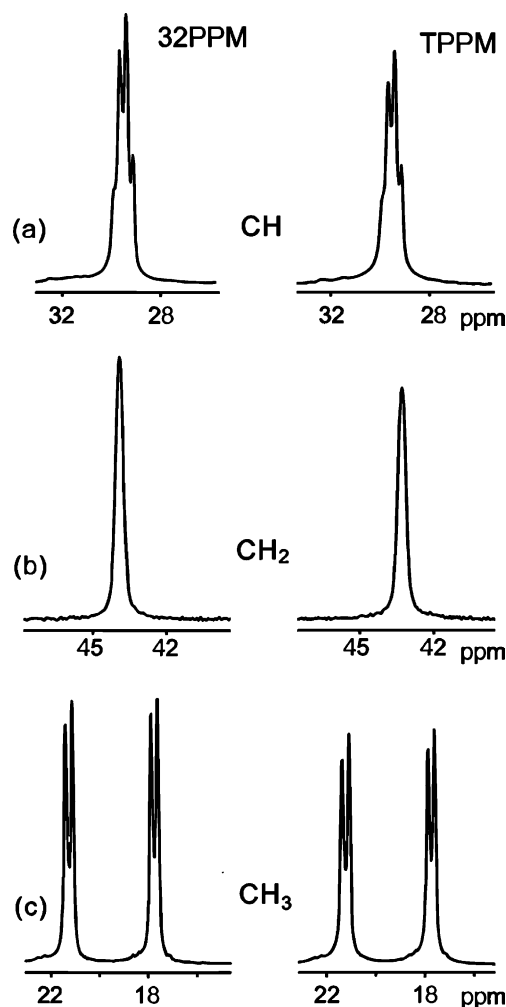


Fig. 5. ^{13}C NMR spectra of CH, CH_2 and CH_3 under the 32PPM and TPPM decoupling pulse sequences. Signals of β carbon (a) and γ carbons (c) of uniformly ^{13}C , ^{15}N labeled valine and α carbon of natural abundance glycine (b) are shown. The J splitting of the center peaks in (a) and that in (c) are 32 and 33 Hz, respectively. The linewidth of the signals in (b) is 43 Hz. The decoupling power 81 kHz, phase excursion angle $2\Phi_0 = 18^\circ$ and the pulse flip angle 170° are the same for the both sequences. The sample spinning frequency was 12.5 kHz.

than CW because CW is a quotient of TPPM at $2\Phi_0 = 0$. In practice, however, it often takes a long time to search even a two-dimensional plane of the TPPM parameters to find the point of maximum performance. As an example, the sequence (Eq. (24)) often shows good results, but it contains three adjustable parameters, and we did not attempt to perform a systematic comparison of its efficiency.

At higher spinning rates, one needs higher decoupling powers to get improvement over the TPPM decoupling. The results displayed in Fig. 6 are similar to that in Fig. 3, but the spinning rate is 14.0 kHz instead of 12.0 kHz. In this case, the increased efficiency of CPM 4-7 and 32PPM is observed at considerably higher decoupling powers.

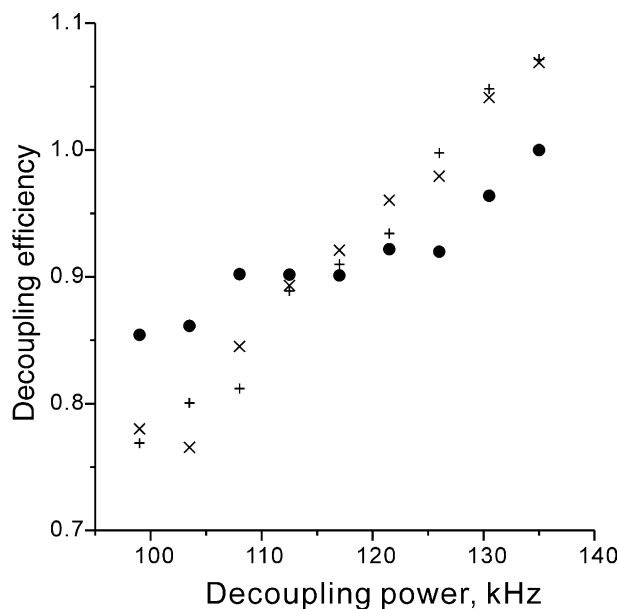


Fig. 6. Decoupling efficiency in glycine of TPPM (●), CPM 4-7 (+), and 32PPM (×) as a function of the decoupling power. The spinning rate is 14.0 kHz.

4. Experiment

The experiments were carried out with a CMX Infinity Plus 500 MHz NMR spectrometer equipped with a Varian broadband double-resonance probe for a 3.2 mm rotor. The spectra in Fig. 6 were recorded with a Varian broadband double-resonance probe for a 4.0 mm rotor. The number of scans was 32 for each spectrum. The polycrystalline glycine was purchased from Sigma (purity >99%) and used without further purification. The uniformly 95% ^{13}C , ^{15}N -labeled L-valine was purchased from Shoko Co. Ltd. Crystals of valine hydrochloride were grown from a dilute hydrochloride solution.

5. Conclusion

The integral of the spectral density of the local field is invariant and cannot be changed by any decoupling sequence. The maximum frequency ω_{rf} , where the center of this spectrum can be "moved" is determined by the available RF power. When the spinning rate ω_r changes from 0 to $\omega_{\text{rf}}/2$, the absorption frequency $2\omega_r$ spans the whole frequency range. Therefore, no universal decoupling scheme can be efficient for a broad range of spinning rates.

At low-to-moderate spinning rates, or when a sufficiently high RF power is available, one can get a significant improvement of the decoupling, compared to TPPM, by using CPM m - n [21], SPINAL-64 [13], or n PPM decoupling sequences. The latter is especially simple in programming and tuning.

Acknowledgments

This work was partly supported by the Grants-in-Aid for Scientific Research on Priority Area from the Ministry of Education, Culture, Sports, Science, and Technology of Japan (H.A. and T.F.), and by grants from the Japan New Energy and Industrial Technology Development Organization and Yokohama City Collaboration of Regional Entities for the Advancement of Technological Excellence, JST (H.A.). A.K. is grateful to the Institute for Protein Research, Osaka University, for hosting him during the summer of 2001, and to Prof. B.M. Fung for helpful and stimulating discussions.

References

- [1] R.R. Ernst, Nuclear magnetic double resonance with an incoherent radio-frequency field, *J. Chem. Phys.* 45 (1966) 3845–3861.
- [2] M.H. Levitt, R. Freeman, Composite pulse decoupling, *J. Magn. Reson.* 43 (1981) 502–507.
- [3] J.S. Waugh, Theory of broadband spin decoupling, *J. Magn. Reson.* 50 (1982) 30–49.
- [4] D. Suter, K.V. Schenker, A. Pines, Theory of heteronuclear decoupling in multispin systems, *J. Magn. Reson.* 73 (1987) 90–98.
- [5] M.H. Levitt, R. Freeman, T.A. Frenkiel, Broadband decoupling in high-resolution nuclear magnetic resonance spectroscopy, *Adv. Magn. Reson.* 11 (1983) 47–110.
- [6] A.J. Shaka, J. Keeler, T. Frenkiel, R. Freeman, An improved sequence for broadband decoupling: WALTZ-16, *J. Magn. Reson.* 52 (1983) 335–338.
- [7] A.J. Shaka, P.B. Barker, R. Freeman, Computer-optimized decoupling scheme for wideband applications and low-level operation, *J. Magn. Reson.* 64 (1985) 547–552.
- [8] T. Fujiwara, K. Nagayama, Composite inversion pulses with frequency switching and their application to broadband decoupling, *J. Magn. Reson.* 77 (1988) 53–63; T. Fujiwara, T. Anai, N. Kurihara, K. Nagayama, Frequency-switched composite pulses for decoupling carbon-13 spins over ultrabroad bandwidths, *J. Magn. Reson. A* 104 (1993) 103–105.
- [9] Z. Starcuk Jr., K. Bartusek, Z. Starcuk, Heteronuclear broadband spin-flip decoupling with variable pulses, *J. Magn. Reson. A* 107 (1994) 24–31; M.R. Bendall, Broadband and narrowband spin decoupling using adiabatic spin flips, *J. Magn. Reson. A* 112 (1995) 126–129; E. Kupce, R. Freeman, Adiabatic pulses for wideband inversion and broadband decoupling, *J. Magn. Reson. A* 115 (1995) 273–276; R. Fu, G. Bodenhausen, Broadband decoupling in NMR with frequency-modulated "chirp" pulses, *Chem. Phys. Lett.* 245 (1995) 415–420.
- [10] B.M. Fung, D.S.L. Mui, I.R. Bonnell, E.L. Enwall, Evaluation of broadband decoupling sequences applied to liquid crystal solutions, *J. Magn. Reson.* 58 (1984) 254–260.
- [11] K.V. Schenker, D. Suter, A. Pines, Broadband heteronuclear decoupling in the presence of homonuclear dipolar and quadrupolar interactions, *J. Magn. Reson.* 73 (1987) 99–113.
- [12] D. Sandström, M.H. Levitt, Structure and molecular ordering of a nematic liquid crystal studied by natural-abundance double-quantum ^{13}C NMR, *J. Am. Chem. Soc.* 118 (1996) 6966–6974.

- [13] B.M. Fung, A.K. Khitrin, K. Ermolaev, An improved broadband decoupling sequence for liquid crystals and solids, *J. Magn. Reson.* 142 (2000) 97–101.
- [14] A.E. Bennett, C.M. Rienstra, M. Auger, K.V. Lakshmi, R.G. Griffin, Heteronuclear decoupling in rotating solids, *J. Chem. Phys.* 103 (1995) 6951–6958.
- [15] D.L. Vanderhart, G.C. Campbell, A close look at ^{13}C CPMAS linewidths in solids for rigid, strongly coupled carbons under CW proton decoupling, *J. Magn. Reson.* 134 (1998) 88–112.
- [16] Z. Gan, R.R. Ernst, Frequency- and phase-modulated heteronuclear decoupling in rotating solids, *Solid State Nucl. Magn. Reson.* 8 (1997) 153–159.
- [17] M. Eden, M.H. Levitt, Pulse sequence symmetries in the nuclear magnetic resonance of spinning solids: application to heteronuclear decoupling, *J. Chem. Phys.* 111 (1999) 1511–1519.
- [18] M. Carravetta, M. Eden, X. Zhao, A. Brinkmann, M. Levitt, Symmetry principles for the design of radiofrequency pulse sequences in the nuclear magnetic resonance of rotating solids, *Chem. Phys. Lett.* 321 (2000) 205–215.
- [19] H. Geen, A.S.D. Heindrichs, J.J. Titman, M. Ernst, B.H. Meier, Investigation of the feasibility of amplitude-modulated dipolar decoupling in magic-angle spinning solid-state nuclear magnetic resonance, *J. Phys. B* 33 (2000) 3377–3391.
- [20] M. Ernst, H. Zimmermann, B.H. Meier, A simple model for heteronuclear spin decoupling in solid-state NMR, *Chem. Phys. Lett.* 317 (2000) 581–588.
- [21] A.K. Khitrin, B.M. Fung, Design of heteronuclear decoupling sequences for solids, *J. Chem. Phys.* 112 (2000) 2392–2398.
- [22] A.K. Khitrin, G. McGeorge, B.M. Fung, Heteronuclear decoupling in solids, in: D.M. Grant, R.K. Harris (Eds.), *Encyclopedia of NMR*, vol. 9, Wiley, Chichester, 2002.
- [23] G. McGeorge, D.W. Alderman, D.M. Grant, Resolution enhancement in ^{13}C and ^{15}N magic-angle turning experiments with TPPM decoupling, *J. Magn. Reson.* 137 (1999) 138–143.
- [24] D.J. Mitchell, J.N.S. Evans, Improved heteronuclear decoupling in REDOR with the use of TPPM, *Chem. Phys. Lett.* 292 (1998) 656–660.
- [25] G. Antonioly, D.E. McMillan, P. Hodgkinson, Line-splitting and broadening effects from F-19 in the C-13 NMR of liquid crystals and solids, *Chem. Phys. Lett.* 344 (2001) 68–74.
- [26] U. Haerberlen, J.S. Waugh, Coherent averaging effects in magnetic resonance, *Phys. Rev.* 175 (1968) 453–467.
- [27] K. Takegoshi, J. Mizokami, T. Terao, ^1H decoupling with third averaging in solid NMR, *Chem. Phys. Lett.* 341 (2001) 540–544.
- [28] M. Ernst, S. Bush, A.C. Kolbert, A. Pines, Second-order recoupling of chemical-shielding and dipolar-coupling tensors under spin decoupling in solid-state NMR, *J. Chem. Phys.* 105 (1996) 3387–3397.
- [29] M. Mehring, in: *Principles of High Resolution NMR in Solids*, Springer, Berlin, 1983, p. 312.
- [30] M. Ernst, A. Samoson, B.H. Meier, Low-power decoupling in fast magic-angle spinning NMR, *Chem. Phys. Lett.* 348 (2001) 293–302.
- [31] A. Bielecki, A.C. Kolbert, M.H. Levitt, Frequency-switched pulse sequences: homonuclear decoupling and dilute spin NMR in solids, *Chem. Phys. Lett.* 155 (1989) 341–346.